Max-Heinrich Laves*, Lüder A. Kahrs, and Tobias Ortmaier

Volumetric 3D stitching of optical coherence tomography volumes

https://doi.org/10.1515/cdbme-2018-0079

Abstract: Optical coherence tomography (OCT) is a non-invasive medical imaging modality, which provides high-resolution transectional images of biological tissue. However, its potential is limited due to a relatively small field of view. To overcome this drawback, we describe a scheme for fully automated stitching of multiple 3D OCT volumes for panoramic imaging. The voxel displacements between two adjacent images are calculated by extending the Lucas-Kanade optical flow algorithm to dense volumetric images. A RANSAC robust estimator is used to obtain rigid transformations out of the resulting flow vectors. The images are transformed into the same coordinate frame and overlapping areas are blended. The accuracy of the proposed stitching scheme is evaluated on two datasets of 7 and 4 OCT volumes, respectively. By placing the specimens on a high-accuracy motorized translational stage, ground truth transformations are available. This results in a mean translational error between two adjacent volumes of $16.6 \pm 0.8\,\mu m$ (2.8 ± 0.13 voxels). To the author's knowledge, this is the first reported stitching of multiple 3D OCT volumes by using dense voxel information in the registration process. The achieved results are sufficient for providing high accuracy OCT panoramic images. Combined with a recently available high-speed 4D OCT, our method enables interactive stitching of hand-guided acquisitions.

Keywords: medical imaging, image processing, registration, panoramic imaging, mosaicing, optical flow

1 Introduction

Optical coherence tomography (OCT) is an imaging modality, which provides high-accuracy cross-sectional information of light scattering biological tissue [8]. The low coherence of a broadband light source allows OCT to perceive microscopic structures in subcutaneous tissue. A major application is examination of the retinal layers in ophthalmology, but OCT is used in a variety of fields, e.g. imaging of vessels, nerves, and other microstructures [15]. Recent advances have enabled the integration of OCT into surgical microscopes, endoscopes, and catheters [9, 17]. However, all of these applications suffer from the relatively small field of view, compared to other cross-sectional modalities (e.g. computed tomography, magnetic resonance imaging, sonography). Often, the structure of interest cannot be captured within a single OCT acquisition. Therefore, this paper deals with automatic stitching of several 3D OCT volumes to generate a single panorama.

The paper is structured as follows: After a short literature review regarding OCT stitching, our approach is presented. We describe the search for correspondences, the estimation of transformations, and how we produce the final volume. Finally, the accuracy is assessed on two different datasets and the validity of our stitching scheme is shown.

1.1 Related Work

Most of the work on registration of 3D OCT focused on 2D registration of planar projections of volumes. With common 2D methods, such as SIFT, the registration of en face or arbitrary projections has already been achieved [5]. Although these approaches consider multiple projections or have an additional depth alignment [14], they do not take dense volumetric information into account.

Merging of 3D OCT volumes has also been achieved by using external navigation data for coarse alignment and additional microscopic images for fine aligment [3]. Using volumetric OCT data, 6 DoF pose estimation has recently been achieved with convolutional neural networks [6]. However, this approach relies on artificial markers in the OCT's field of view and does not focus on registration between the volumes. Also considering volumetric information, accurate registration of two OCT volumes has been done by extending SIFT to 3D [13].

2 Materials and Methods

2.1 Image acquisition

In order to generate adjacent overlapping 3D OCT volumes with known displacements, two specimens are consecutively placed on a motorized linear stage (MZ812B, ThorLabs Inc.,

***Corresponding author: Max-Heinrich Laves,** Institute of Mechatronic Systems, Appelstr. 11A, 30167 Hannover, Germany, e-mail: laves@imes.uni-hannover.de
Lüder A. Kahrs, Tobias Ortmaier, Institute of Mechatronic Systems, Appelstr. 11A, 30167 Hannover, Germany

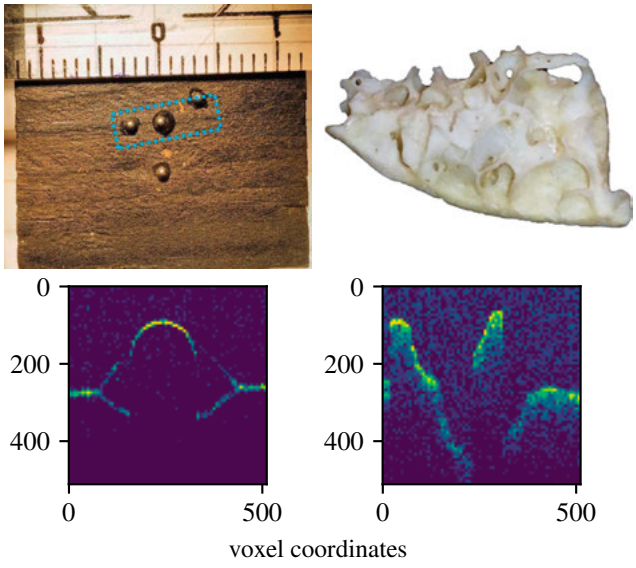

Fig. 1: Specimens, left: *sphere board* with marked OCT scan area, right: human *temporal bone*, bottom row: exemplary OCT B-scans.

Newton, NJ, USA) with a repeatability of 1.5 µm and are captured by a swept-source OCT (OCS1300SS, ThorLabs Inc., lateral resolution 12 µm). The first specimen is a wooden board with metal spheres glued on it (named *sphere board* in the following) and the second specimen is a small piece of human *temporal bone* (see Fig. 1). The scan dimensions are equally set to 3 mm for each spatial direction with a resolution of 512 voxels. This results in isotropic voxels with an edge size of 6 µm. The *sphere board* specimen is captured 7 times and the *temporal bone* specimen 4 times, each with translations of 0.75 mm by the linear stage.

2.2 Extending Lucas-Kanade

For estimating voxel displacements between two adjacent and overlapping OCT volumes of the same object, the forward additive Lucas-Kanade optical flow method is used [1]. The extension of the algorithm to a third dimension in order to use it on dense 3D voxel data has already been achieved for ultrasonic volumes [12] and is shortly revised in the following.

Optical flow is referred to as the parameters $\boldsymbol{p}$ of a warp function

$$\boldsymbol{W}(\boldsymbol{x}, \boldsymbol{p}) = \begin{pmatrix} x + p_0 \\ y + p_1 \\ z + p_2 \end{pmatrix} \tag{1}$$

aligning a template volume $\boldsymbol{T}(\boldsymbol{x})$ onto an input volume $\boldsymbol{I}(\boldsymbol{x})$ with the voxel coordinates $\boldsymbol{x} = (x, y, z)^\intercal$. The template $\boldsymbol{T}$ is a volume patch with a size of e.g. $7 \times 7 \times 7$ voxels extracted from the first of the two volumes. Finding these parameters results in minimizing the sum of squared errors

$$\arg\min_{\Delta \boldsymbol{p}} \sum_{\boldsymbol{x}} [\boldsymbol{I}(\boldsymbol{W}(\boldsymbol{x}, \boldsymbol{p} + \boldsymbol{\Delta p})) - \boldsymbol{T}(\boldsymbol{x})]^2 \tag{2}$$

between the template and the warped input volume with respect to incremental parameter updates $\Delta \boldsymbol{p}$ with $\boldsymbol{p} \leftarrow \boldsymbol{p} + \Delta \boldsymbol{p}$. This is repeated iteratively until convergence with $\|\Delta \boldsymbol{p}\| < \varepsilon$ or until a maximum number of iterations is reached. Equation 2 is solved by linearizing with first-order Taylor series, which results in a least squares problem with closed form solution. It can be solved by derivation with respect to $\Delta \boldsymbol{p}$. For more details, please refer to [1].

Choosing a small window size for sampling the template $\boldsymbol{T}$ generally relates to high accuracy, as details are not "smoothed out" when integrating the erros in Eq. 2. However, this has a negative effect on the robustness when undergoing large motions, where a large window size is preferred. To overcome this compromise, we are extending our 3D implementation of Lucas-Kanade with a pyramid approach inspired by [2].

With our pyramidal approach, the window size is kept constantly small. A volume pyramid is created for each of two adjacent volumes by repeatedly Gaussian smoothing and subsampling by a factor of 2. The iterative minimization of Eq. 2 is started at the highest pyramid level with lowest resolution. After convergence, the result of this is multiplicated by the subsampling factor and used as initialization for the next pyramid level. Therefore, it is essential for the algorithm to be operated with sub-voxel accuarcy. To obtain intensities at non-integer voxel coordinates, we use multivariate linear interpolation.

2.3 Volume stitching

The final volume stitching is performed as follows. Prior to calculating the optical flow, we identify distinct, good to track volume keypoints by exploiting the Harris corner detector [7], also extended to 3D. At the local maxima of the Harris response we calculate the optical flow as described above. For every flow vector, the matching error (given by evaluating Eq. 2 at found $\boldsymbol{p}$) is used to keep the best 50 % matches.

The actual stitching is performed by transforming voxel coordinates of subsequent volumes into the coordinate frame of the first one and adding their voxel intensities. For this, we assume a rigid transformation between two volumes i and $i+1$, which is estimated by an outlier-robust RANSAC estimator [4]. This results in $n-1$ transformation matrices ${}^{i}\boldsymbol{A}_{i+1}$ for n volumes.

After transforming all volumes, a blending of overlapping areas is performed. We find those areas by logical conjunction of all non-zero voxels before adding them together. The

final voxel intensity is the mean of two overlapping intensities. Additionally, more elaborated blending can be done by linear interpolation of intensities at sub-voxel level.

3 Experimental results

With a window size of $5 \times 5 \times 5$ voxels, 5 pyramid levels and $\varepsilon = 1 \cdot 10^{-3}$ promising results can be achieved. The RANSAC confidence interval is initially set to 0.5 voxels, but dynamically increased by steps of 0.5 voxels, if not enough inliers are found. Qualitative results of the *sphere board* and *temporal bone* dataset are shown in Fig. 2. For better visualization, the surfaces of the specimens have been reconstructed by using the marching cubes algorithm [11]. The resulting panoramic volumes are valid and reveal a high-resolution dense 3D acquisition of otherwise imperceptible objects (see Fig. 3). A small misalignment can be seen in the left third of the *sphere-board*. This can be explained by the planar, feature-less surface in this area.

Due to placing the specimens on a motorized linear stage during OCT acquisition, ground truth transformation values are available. The *sphere board* dataset is shifted 0.75 mm in x-direction between each volume and the *temporal bone* dataset is shifted -0.75 mm in z-direction, respectively. To assess for accuracy and taking rotation errors into account, the center voxel coordinate $\boldsymbol{x}_c = (256, 256, 256)^\intercal$ is transformed by each estimated transformation ${}^{i}\boldsymbol{A}_{i+1}$, resulting in $\boldsymbol{x}'_c = {}^{i}\boldsymbol{A}_{i+1}^{-1}\, \boldsymbol{x}_c$. The error to ground truth is then defined as

$$e_i = \left| 750\,\mu\text{m} - 6\,\mu\text{m}\,\text{voxels}^{-1} \cdot \|\boldsymbol{x}_c - \boldsymbol{x}'_c\|_2 \right| . \qquad (3)$$

Error values for each volume pair of the two datasets are listed in Tab. 2. Both mean errors are in the same order of magnitude as the OCT's lateral resolution, whereby the *temporal bone* dataset is stitched slightly more accurate. The runtimes of the individual calculation steps of the implementation are listed in Tab. 1.

Tab. 1: Runtimes in seconds of all steps of the automated stitching for the temporal bone dataset with $256 \times 256 \times 256$ voxels on an Intel Core i9-7900X CPU (Intel Corp., Santa Clara, CA, USA) with CPython 3.6.4 interpreter.

vol	data loading	Harris corner	optical flow	RANSAC
0→1	2.51	7.65	68.0	0.19
1→2	2.60	4.64	80.8	0.19
2→3	2.56	4.60	64.2	0.18
sum	7.67	16.9	213	0.56

Tab. 2: Error values e_i of transformations in µm for each dataset.

dataset	0→1	1→2	2→3	3→4	4→5	5→6	mean
s. board	22.6	21.4	19.5	19.3	23.2	22.8	21.5
t. bone	15.7	17.6	16.5	n/a	n/a	n/a	16.6

4 Conclusion

We present an automated registration and stitching of 3D OCT volumes with voxel accuracy. Our stitching scheme is based on 3D optical flow and RANSAC estimation of rigid transformations between volumes. In contrast to previous approaches, we use dense volumetric information and concatenate any number of volumes. Stitching overcomes the disadvantages of small scan volumes by enabling the imaging of larger areas.

Current state-of-the-art high-speed OCT devices can operate at 25 volumes per second [18]. To adapt to those volume rates for live stitching, future work aims on implementing the Harris corner detector and the Lucas-Kanade algorithm in a parallel manner on a GPGPU. We also consider on extending the algorithm to non-rigid transformations. This enables the tracking of soft tissue areas (e.g. vocal folds), which we have already achieved on stereo camera images [16]. The optical flow can also be used for volume of interest stabilization in 4D OCT [10].

Acknowledgment: The authors thank Christian van Kempen for his initial experiments and implementation.

Author Statement

Research funding: This research has received funding from the European Union as being part of the ERFE OPhonLas project. Conflict of interest: The authors state no conflict of interest. Informed consent: Informed consent is not applicable. Ethical approval: For this kind of study ethical approval is not required.

References

[1] S. Baker and I. Matthews. Lucas-kanade 20 years on: A unifying framework. *International Journal of Computer Vision*, 56(3): 221–255, Feb 2004. 10.1023/B:VISI.0000011205.11775.fd.

[2] J.-Y. Bouguet. Pyramidal implementation of the lucas kanade feature tracker. *Intel Corporation, Microprocessor Research Labs*, 2000.

[3] M. Finke, S. Kantelhardt, A. Schlaefer, R. Bruder, E. Lankenau, A. Giese, and A. Schweikard. Automatic scanning of large tissue areas in neurosurgery using optical coherence tomography. *Int. J. Med. Rob. Comput. Assist. Surg.*, 8(3):327–336. 10.1002/rcs.1425.

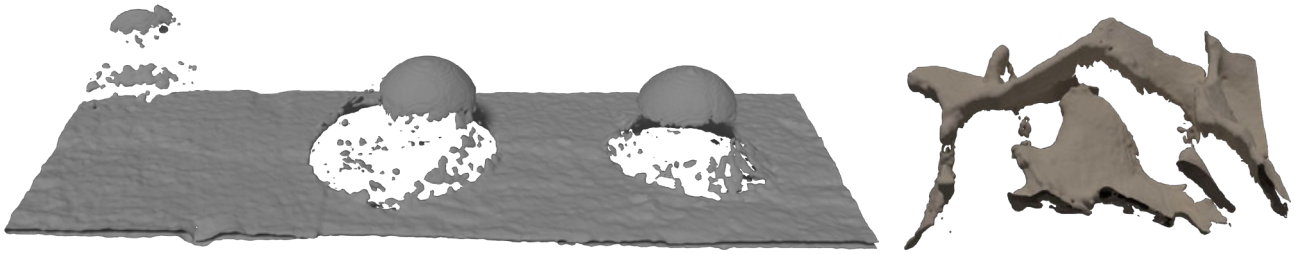

Fig. 2: Rendering of stitched *sphere board* (left) and *temporal bone* (right) datasets. For better visualization, the surfaces have been reconstructed.

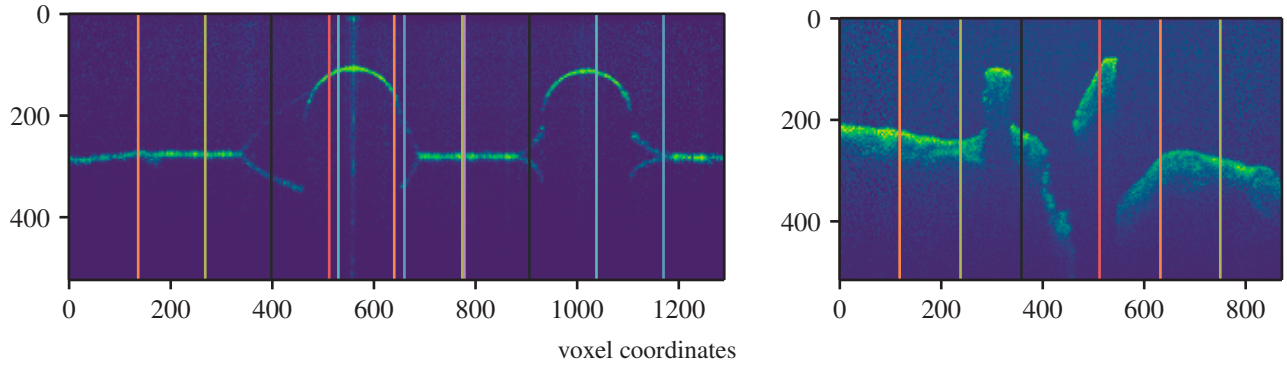

Fig. 3: OCT slices of stitched *sphere board* (left) and *temporal bone* (right) datasets. The boundaries of the individual volumes are highlighted by colored dashed lines.

[4] M. A. Fischler and R. C. Bolles. Random sample consensus: A paradigm for model fitting with applications to image analysis and automated cartography. *Commun. ACM*, 24(6):381–395, June 1981. 10.1145/358669.358692.

[5] Y. Gan, W. Yao, K. M. Myers, and C. P. Hendon. An automated 3D registration method for optical coherence tomography volumes. In *Proc. of Int. Conf. IEEE Eng. Med. Biol. Soc.*, pages 3873–3876, 2014. 10.1109/EMBC.2014.6944469.

[6] N. Gessert, M. Schlüter, and A. Schlaefer. A deep learning approach for pose estimation from volumetric OCT data. *Medical Image Analysis*, 46:162–179, 2018. 10.1016/j.media.2018.03.002.

[7] C. Harris and M. Stephens. A combined corner and edge detector. In *Proc. of Fourth Alvey Vision Conference*, volume 15, pages 10–5244, 1988.

[8] D. Huang, E. A. Swanson, C. P. Lin, J. S. Schuman, W. G. Stinson, W. Chang, M. R. Hee, T. Flotte, K. Gregory, C. A. Puliafito, and J. G. Fujimoto. Optical coherence tomography. *Science*, 254 (5035):1178–1181, 1991. 10.1126/science.1957169.

[9] E. Lankenau, D. Klinger, C. Winter, A. Malik, H. H. Müller, S. Oelckers, H.-W. Pau, T. Just, and G. Hüttmann. Combining Optical Coherence Tomography (OCT) with an Operating Microscope. In *Adv. Med. Eng.*, pages 343–348, 2007. 10.1007/978-3-540-68764-1_57.

[10] M.-H. Laves, A. Schoob, L. A. Kahrs, T. Pfeiffer, R. Huber, and T. Ortmaier. Feature tracking for automated volume of interest stabilization on 4D-OCT images. In *Proc. SPIE*, volume 10135, pages 10135–10135–7, 2017. 10.1117/12.2255090.

[11] W. E. Lorensen and H. E. Cline. Marching cubes: A high resolution 3d surface construction algorithm. In *Proc. of 14th Annual Conference on Computer Graphics and Interactive Techniques*, pages 163–169, New York, NY, USA, 1987. ACM. 10.1145/37401.37422.

[12] J. Meunier. Tissue motion assessment from 3D echographic speckle tracking. *Phys Med. Biol.*, 43(5):1241–1254, 1998.

[13] M. Niemeijer, M. K. Garvin, K. Lee, B. van Ginneken, M. D. Abràmoff, and M. Sonka. Registration of 3D spectral OCT volumes using 3D SIFT feature point matching. In *Proc. SPIE*, volume 7259, pages 72591I–72591I–8, 2009. 10.1117/12.811906.

[14] M. Niemeijer, K. Lee, M. K. Garvin, M. D. Abràmoff, and M. Sonka. Registration of 3D spectral OCT volumes combining ICP with a graph-based approach. In *Proc. SPIE*, volume 8314, pages 8314–8314–9, 2012. 10.1117/12.911104.

[15] J. M. Schmitt. Optical Coherence Tomography (OCT): A Review. *IEEE Journal of Selected Topics in Quantum Electronics*, 5(4): 1205–1215, Jul 1999. 10.1109/2944.796348.

[16] A. Schoob, M.-H. Laves, L. A. Kahrs, and T. Ortmaier. Soft tissue motion tracking with application to tablet-based incision planning in laser surgery. *Int. J. Comput. Assist. Radiol. Surg.*, 11(12):2325–2337, 2016. 10.1007/s11548-016-1420-5.

[17] G. J. Tearney, S. A. Boppart, B. E. Bouma, M. E. Brezinski, N. J. Weissman, J. F. Southern, and J. G. Fujimoto. Scanning single-mode fiber optic catheter–endoscope for optical coherence tomography. *Opt. Lett.*, 21(7):543–545, Apr 1996. 10.1364/OL.21.000543.

[18] W. Wieser, W. Draxinger, T. Klein, S. Karpf, T. Pfeiffer, and R. Huber. High definition live 3D-OCT in vivo: design and evaluation of a 4D OCT engine with 1 GVoxel/s. *Biomed. Opt. Express*, 5(9):2963–2977, 2014. 10.1364/BOE.5.002963.